# FEATURE ARTICLE

## Acetylene at the Threshold of Isomerization

### Matthew P. Jacobson and Robert W. Field*

*Department of Chemistry and George R. Harrison Spectroscopy Laboratory, Massachusetts Institute of Technology, Cambridge, Massachusetts 02139*

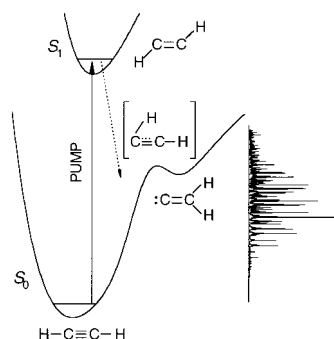*Received: July 15, 1999; In Final Form: November 10, 1999*

This article reviews recent research on acetylene which is intended as a contribution to the understanding of intramolecular vibrational energy flow when it is poorly described by either statistical (i.e., RRKM) or purely separable (i.e., harmonic oscillator/normal mode) models. The experimental spectra that inform this investigation are $\sim 7$ cm$^{-1}$ resolution dispersed fluorescence spectra of the acetylene $S_1 \rightarrow S_0$ system. Above 10 000 cm$^{-1}$ of vibrational energy, these spectra are extremely congested and cannot be analyzed using conventional spectroscopic assignment procedures. Instead, a numerical pattern recognition procedure is utilized to disentangle spectroscopic patterns that are associated with approximately conserved polyad quantum numbers. This pattern recognition analysis makes possible detailed modeling of the short-time ($\sim 1$ ps) but large-amplitude vibrational dynamics of acetylene at high energy (15 000 cm$^{-1}$), which is demonstrated here to be dominated by regularity even for the low-frequency bending motions (22 quanta of bend excitation). That is, a few stable motions dominate the large-amplitude bending dynamics, including *local bend* (one hydrogen bending), which is closely related to the acetylene-vinylidene isomerization coordinate, and a new type of vibrational motion that we call *counter-rotation*, in which the two hydrogens undergo circular motions on opposite ends of the CC core.

## I. Introduction

The work reported in this article is intended as a contribution toward the understanding of the vibrational dynamics of small polyatomic molecules when they have sufficient vibrational energy to sample regions of the potential energy surface that are far from equilibrium. At the simplest level, the motivation for such research is the fact that bond-breaking chemical reactions do not occur near equilibrium and necessarily involve highly vibrationally excited reactants and/or products. Many issues related to large-amplitude vibrational dynamics remain unresolved, but a particularly central one is the extent to which such dynamics can be described as chaotic, in which case statistical models are appropriate, or regular, in which case there exist approximately conserved (i.e., not guaranteed by any rigorous symmetry) constants of motion.

* To whom correspondence should be addressed.

For many years acetylene has served as a prototype molecule for studies of large-amplitude vibrational motion because it is one of the simplest possible bond-breaking isomerizing systems. The isomerization in question is from the stable, linear ($D_{\infty h}$) isomer of acetylene to the quasi-stable vinylidene ($C_{2v}$) structure, and requires over 15 000 cm$^{-1}$ (nearly 2 eV, or 43 kCal/mol) of internal excitation, as predicted by ab initio calculations[1-6] (see Figure 1 for a schematic representation). In this article, we describe recent experimental and theoretical investigations of the vibrational dynamics of acetylene up to excitation energies *just below* the threshold of isomerization (i.e., up to 15 000 cm$^{-1}$). At such an energy, the molecule is capable of undergoing very large amplitude vibrational motions, and we demonstrate that there exists substantial experimental evidence for a particular type of vibrational motion called "local bend", in which the molecule samples the isomerization coordinate and (in a

**Figure 1.** Schematic representation of the ground and first excited singlet states of acetylene. The most stable configuration of acetylene in its ground electronic state is linear, but vinylidene exists as a quasi-stable species whose zero-point level lies ~15 200 cm$^{-1}$ above the linear zero point.[6] The transition state for the acetylene-vinylidene isomerization has a half-linear structure. The zero-point level of the trans bent first excited singlet state lies at ~42 200 cm$^{-1}$. The spectrum on the right is the origin band DF spectrum.[20]

classical sense) spends much more time near the isomerization transition state than it does near the equilibrium configuration. Although in this article we focus on our recent work at MIT, it should be emphasized that other research groups have contributed substantially to the emerging understanding of large-amplitude vibrations in acetylene; we are particularly indebted to Profs. K. Yamanouchi (University of Tokyo)[7,8] and M. Herman (University Libre de Bruxelles)[9−11] for their contributions, which have strongly and directly impacted our own.

This article will be organized around the experimental and theoretical challenges that arise when attempting to study a molecule when it has nearly enough energy to isomerize. With respect to experiment, the frequency domain spectra of even relatively small polyatomics such as acetylene tend to be quite congested at high vibrational energy, due to the necessarily high density of vibrational states, and complex, due to the energetic accessibility of far-from-equilibrium regions of the potential surface. However, we have found that for acetylene, a *numerical pattern recognition* analysis permits an essentially complete assignment of the ~5 cm$^{-1}$ resolution experimental spectra up to at least the energy of the isomerization transition state. Although our extensive use of numerical, automated algorithms for spectrum analysis is novel, the essence of our pattern recognition approach is not. On the contrary, (visual) pattern recognition lies at the heart of all traditional methods of spectrum interpretation. Simple examples of spectroscopic patterns include *P*, *Q*, and *R* rotational branches or Franck−Condon vibrational progressions; in each case, the existence of patterns is associated with rigorously or approximately conserved quantum numbers (rotational in the former case and vibrational in the latter). When these quantum numbers become locally nonconserved, for instance due to anharmonic or Coriolis resonances, then the usual spectroscopic patterns are corrupted (perturbed) in some way. In the most extreme case, the destruction of all nonrigorously conserved quantum numbers is associated with classical chaos (and its quantum manifestations);[12] if a molecule could be studied that approaches this "bag of atoms" limit[13] at sufficiently high internal energy, one would expect to be unable to identify any spectroscopic patterns (except perhaps those based upon rigorous symmetries, such as parity and total angular momentum), and the only insights to be gained would be statistical in nature.

Acetylene, however, does not even remotely approach this bag-of-atoms limit at 15 000 cm$^{-1}$ of vibrational excitation, and

our numerical pattern recognition analysis proceeds by identification of patterns associated with approximately conserved quantities called polyad quantum numbers (see section II), which are generalizations of the traditional normal mode quantum numbers. The partitioning of the acetylene spectra into these polyad patterns is the crucial first step in the analysis, but the patterns themselves encode the ball-and-spring dynamics of the molecule in complicated ways, and a model is needed to extract from the patterns a simple physical picture of the large-amplitude molecular vibrations. The model that we employ is a standard quantum mechanical *effective Hamiltonian*. Such models are typically associated with the analysis of the spectra of molecules near equilibrium, and with long lists of spectroscopic constants which may not have any obvious physical interpretation. However, effective Hamiltonian models are not only capable of accurately reproducing experimental spectra at high vibrational energy, but can also provide tremendous physical insights into the vibrational motions, particularly through a combination of quantum mechanical and (semi)classical analysis. In the case of acetylene, this analysis reveals that the unimolecular vibrational dynamics of acetylene with up to 15 000 cm$^{-1}$ of vibrational energy is dominated by regularity even for the low frequency bending modes (15 000 cm$^{-1}$ corresponds to 22 quanta of bend excitation!). That is, a few stable vibrational motions dominate the dynamics, although these stable motions are generally unrelated to the normal mode motions that dominate the low energy dynamics. These stable large-amplitude motions include local bend (one hydrogen bending) and a new type of vibrational motion that we call counter-rotation (the two hydrogens undergoing circular motions on opposite ends of the CC core).

## II. DF Spectra

The acetylene ground electronic state has previously been, and continues to be, extensively characterized by absorption spectroscopy, which is sensitive primarily to CH stretch excitation (see refs 9 and 11 for a review of available acetylene absorption data). However, as Figure 1 makes clear, the acetylene−vinylidene isomerization is more closely related to the bending and CC stretch motions of acetylene than to the CH stretch motions, since during the course of the isomerization one hydrogen must move to the other end of the CC core, and the CC bond must be converted from a triple to a double bond. To obtain spectroscopic data more directly relevant to acetylene-vinylidene isomerization, the MIT group has for many years[14−18] recorded double resonance spectra of acetylene using rovibrational levels of the $S_1$ state as intermediates. The majority of these experiments have utilized the stimulated emission pumping (SEP) technique,[19] in which a PUMP laser populates single systematically selected rovibrational levels of the acetylene $S_1$ state, and a DUMP laser stimulates emission back down to excited rovibrational levels of the $S_0$ state. The large geometry change between the $S_0$ and $S_1$ states allows the DUMP transitions to probe the $S_0$ surface at rather high internal energies (up to at least 28 000 cm$^{-1}$). In particular, the Franck−Condon principle implies that, since the $S_1$ state has a trans bent geometry with a nominal CC double bond, $S_0$ vibrational levels with excitation in the CC stretch and trans bend modes will be particularly prominent in the double resonance spectra.

More recently, the SEP studies of acetylene have been complemented by dispersed fluorescence (DF) spectra. The DF experiments differ from SEP in that a DUMP laser is not used. Instead, the intensity of the spontaneous emission is recorded as a function of wavelength using a monochromator and an appropriate detector. See Refs 14 and 20−22 for details of the

Feature Article

*J. Phys. Chem. A, Vol. 104, No. 14, 2000* **3075**

**TABLE 1.**

| mode | motion |
|---|---|
| $\nu_1$ | symmetric CH stretch |
| $\nu_2$ | CC stretch |
| $\nu_3$ | antisymmetric CH stretch |
| $\nu_4$ | trans bend |
| $\nu_5$ | cis bend |
| $l_4/l_5$ | vibrational angular momentum |

methodology employed to record and calibrate (both frequency and intensity) our DF spectra. It should be noted that the original origin band DF spectrum was recorded at Hope College in collaboration with Prof. William Polik.[20] The groups of Profs. Tsuchiya[7,23,24] and Yamanouchi[8] have also recorded dispersed fluorescence spectra of acetylene, and their original study in fact motivated the subsequent DF studies in our group. The DF spectra that have been recorded from the $S_1$ state of acetylene have much lower resolution (poorer than 4 cm$^{-1}$) than the SEP spectra, in which the resolution is limited by the DUMP laser bandwidth, which is $\sim$0.05 cm$^{-1}$ for typical commercial dye laser systems. The decreased resolution of the DF spectra makes it possible to map out large regions of the $S_0$ potential surface much more rapidly than is possible with SEP, although it of course also limits the level of spectroscopic detail. However, from the standpoint of understanding unimolecular dynamics, low resolution corresponds to short-time dynamics, which must be fully characterized before any attempt is made to describe the longer time dynamics encoded by higher resolution spectra. In addition, for polyatomic molecules at high internal energy, the short time (a few picoseconds) dynamics are rarely simple and can provide a wealth of information about the molecular potential energy surface.

Extracting the short-time but large-amplitude dynamics of acetylene from the complex DF spectra (see Figure 1) represents a substantial challenge for spectrum interpretation. In the case of the acetylene DF spectra, regular vibrational progressions can only be observed at rather low internal energy ($\lesssim$7000 cm$^{-1}$). At higher energies, the anharmonicities in the potential surface lead to strong anharmonic couplings among the normal mode states (note that Coriolis resonances play a very minor role in our spectra, which sample low rotational quantum numbers, $J \leq 2$). The resultant rapid and extensive intramolecular vibrational redistribution (IVR) implies that the normal mode quantum numbers are no longer even approximately conserved and that traditional spectroscopic assignment will be unsuccessful. However, the existence of strong anharmonic resonances does not imply that all vibrational quantum numbers become nonconserved. In particular, Fried and Ezra,[25] and Kellman,[26-28] have demonstrated that, given a set of dynamically important anharmonic resonances, certain generalized vibrational quantum numbers, called polyad numbers, may remain conserved (the term "polyad" is also used to refer collectively to all states with the same set of polyad numbers). In the case of acetylene, the 11 anharmonic resonances[9,10,20] that have been identified, primarily through $S_0$ state absorption spectroscopy, imply the existence of three conserved polyad numbers:[26-28]

$$N_{res} = 5\nu_1 + 3\nu_2 + 5\nu_3 + \nu_4 + \nu_5 \qquad (1)$$

$$N_s = \nu_1 + \nu_2 + \nu_3 \qquad (2)$$

$$l = l_4 + l_5 \qquad (3)$$

where the normal node notation for acetylene is shown in Table 1.

The physical meanings of the $N_s$ and $l$ quantum numbers are simple; they represent the total number of quanta of stretching excitation and the total vibrational angular momentum, respectively. The $N_{res}$ quantum number has a slightly more subtle meaning; it reflects the approximate ratios among the normal-mode frequencies and thus represents a restriction under which only states with approximately the same zero-order energy may interact. That is, near-degeneracies among the zero-order states can be predicted by the frequency ratios among the normal modes, and the anharmonic resonances that couple these nearly degenerate groups of states are those that play a dominant role in the short-time dynamics. It should be emphasized that polyad-nonconserving anharmonic resonances are guaranteed to exist. However, as discussed in section IV, our results, as well as the many absorption studies,[11] provide strong evidence that these resonances play at most a minor role in the short-time (several picoseconds) dynamics, and thus that the polyad numbers remain approximately conserved, up to at least 15 000 cm$^{-1}$.

Our analysis of the acetylene DF spectra is based upon identifying spectroscopic patterns associated with the polyad numbers. That is, each polyad is associated with a spectroscopic pattern, and the various polyad patterns are related to each other by simple (harmonic oscillator) scaling rules for the diagonal and off-diagonal matrix elements (see section IV). As a practical matter, however, identification of the polyad patterns in any single DF spectrum is made difficult by overlap between adjacent patterns, as well as by finite resolution and signal-to-noise ratio. Our pattern recognition analysis proceeds by comparing *multiple* DF spectra that are recorded using different vibrational levels of the $S_1$ state. This unconventional approach is made possible by the fact that the zero-order states that are bright in our DF spectra, (0, $\nu_2$, 0, $\nu_4$, 0), (i.e., those involving excitation in only the CC stretch and trans bend modes) are distributed such that there exists at most one bright state in each polyad.[20] This fact implies that no interference effects will be observed between different bright states. That is, each bright state fractionates into a unique set of dark states; conversely, each eigenstate gains intensity from only one zero-order bright state. The absence of interference effects between the bright states implies that each bright state must display the same fractionation pattern in each of the DF spectra, regardless of which vibrational level of $S_1$ was utilized as an intermediate. Within any spectrum, the absolute intensity of a fractionation pattern, born from a single bright state, arises from a unique Franck−Condon factor (namely that connecting the selected upper level to the single bright state). That is, each DF spectrum contains the same fractionated bright state patterns but with different absolute intensities, and the fractionated bright state patterns can be identified through cross-comparisons of the relative intensities in multiple DF spectra.

Figure 2 depicts three dispersed fluorescence spectra, which were recorded using the $S_1$ origin band (dashed line), $2\nu_3'$ band (solid line), and $\nu_2'+2\nu_3'$ (dotted line) band, in the 14 000−15 000 cm$^{-1}$ region, i.e., just below the threshold of isomerization [note that in the $S_1$ state, $\nu_2'$ is the CC stretch mode, and $\nu_3'$ is the trans bend]. It should be noted that in each case the DF spectra were recorded using a $^rQ_0(1)$ absorption line, which leads to a two-line rotational pattern in emission, consisting of transitions terminating on ($J = 1$, $l = 0$) and ($J = 2$, $l = 2$) levels of the $S_0$ state. Thus, each fractionation pattern that can be identified in the spectra arises from a pair of bright states, (0, $\nu_2$, 0, $\nu_4^0$, 0°) and (0, $\nu_2$, 0, $\nu_4^2$, 0°). This extra rotational structure in the fractionation patterns poses few problems for the analysis presented below.
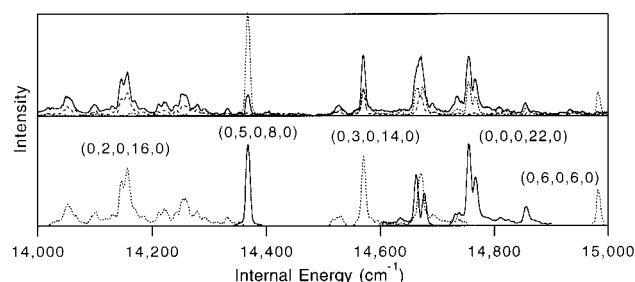
**Figure 2.** Top: Three dispersed fluorescence spectra, which were recorded using the origin band (dashed line), $2\nu_3'$ band (solid line), and $\nu_2' + 2\nu_3'$ (dotted line) band. Bottom: Five fractionated bright states can be identified in this region, using our pattern recognition scheme. The (0, 2, 0, 16, 0) bright state can be easily identified by eye because it happens not to overlap substantially with any other fractionated bright states. However, the ability to identify bright states visually is the exception rather than the rule at high energy, and numerical pattern recognition (XCC) permits the disentanglement of overlapped bright states, such as (0, 3, 0, 14, 0) and (0, 0, 0, 22, 0).

Five fractionated bright state patterns can be identified in the $14\,000-15\,000\ cm^{-1}$ region, and these are displayed below the raw spectra. The two patterns in the region below $14\,400\ cm^{-1}$ are particularly easy to identify. The first zero-order bright state, (0, 2, 0, 16, 0), has significant Franck–Condon factors in the $2\nu_3'$ (solid line) and origin (dashed line) band DF spectra and is fractionated over an energy region at least $300\ cm^{-1}$ wide. That is, this fractionated bright state can be identified because the emission patterns from the $2\nu_3'$ and origin bands are nearly identical (other than a constant multiplicative factor) from $14\,000\ cm^{-1}$ to $14\,300\ cm^{-1}$. The sharp peak near $14,350\ cm^{-1}$ clearly belongs to a different fractionated bright state because its ratio of intensities among the three spectra is strikingly different from that of the peaks in the $14\,000-14\,300$ region. The zero-order bright state that illuminates this peak has a relatively large Franck–Condon factor in the $\nu_2' + 2\nu_3'$ spectrum (dotted line), and can be assigned to be (0, 5, 0, 8, 0).

## III. XCC

The ability to identify fractionated bright states by eye is the exception rather than the rule at high internal energy; the region $14\,000-14\,500\ cm^{-1}$ is anomalous, in the sense that systematic and often severe overlap between bright states is observed in most other energy regions. The energy range $14\,500-15\,000\ cm^{-1}$ is more typical. In this region, it is difficult to ascertain *visually* even how many fractionated bright states are present. Due to the ubiquity of such difficult regions, we have developed and employed a *numerical* pattern recognition technique to identify fractionated bright states.

The numerical spectroscopic pattern recognition technique that we employ is called the eXtended Cross Correlation (XCC),[29–31] which we developed in collaboration with Dr. Stephen Coy (MIT). To introduce the XCC and illustrate its properties, we define in Figure 3 a simple synthetic data set. Specifically, the top panels of Figure 3 depict two patterns (which could represent, for instance, two fractionated bright states) and two synthetic spectra that are generated by taking distinct linear superpositions of the patterns. That is,

$$I_1(x) = a_1 I_A(x) + b_1 I_B(x) \tag{4}$$

$$I_2(x) = a_2 I_A(x) + b_2 I_B(x) \tag{5}$$

Note that numbers are used to label spectra, and letters to label patterns. The parameter "$x$" in a real experimental spectrum
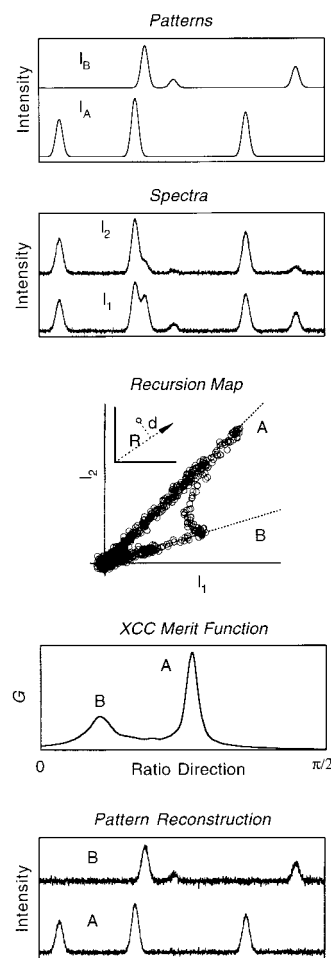


**Figure 3.** The XCC technique is illustrated using synthetic spectra. The spectra in the second panel are constructed as linear combinations of the patterns in the top panel, with superimposed Gaussian random noise. Each point on the recursion map (middle part) represents the intensities in the two spectra at the same frequency. The inset shows the $(R,d)$ coordinates that are used to define the XCC merit function, and ratio directions optimized from the merit function are shown as dotted lines. The XCC merit function (eq 10) is depicted in the fourth panel, with the ratio direction represented by the angle between the fit line and the $x$-axis in the recursion map. The ratio directions optimized using the merit function can be used to reconstruct the patterns from the spectra (bottom part), using eqs 11 and 12.

would represent (for example) frequency, wavelength, or internal energy. For the synthetic example, the $x$-axis will be referred to as frequency, without loss of generality. The coefficients $a_1$, $a_2$, $b_1$, and $b_2$ describe the amplitudes of the patterns in each spectrum, and in this particular example have the values of 1.00, 1.11, 1.00, and 0.33, respectively. In addition, to make the spectra resemble real, experimental data sets, Gaussian random noise is superimposed upon each of the synthetic spectra.

Understanding the point of view used in the XCC requires some mental gymnastics to invert the way in which the experimental data is organized. A spectroscopic data set is conventionally regarded as a group of spectra, each of which consists of a set of (usually discrete) measurements. The XCC regards a spectroscopic data set as groups of measurements, each of which is made in all spectra at a single frequency. To make this idea concrete, a *recursion map*[92] is defined the middle panel of Figure 3 for the two synthetic spectra. The recursion map in this case is two-dimensional, with the coordinates representing the intensity values in the two spectra. That is, the coordinates of each point represent the intensities in the two

Feature Article

*J. Phys. Chem. A, Vol. 104, No. 14, 2000*  **3077**

spectra at a given frequency. Thus, no information about frequency appears on the recursion map.

The points on the recursion map can be categorized as follows.

**1. Points near the Origin.** These points correspond to frequencies at which both spectra have low intensities. The scatter of these points about the origin is due to the noise in the spectra.

**2. Points That Cluster about "Rays" That Pass through the Origin.** The points that scatter about these rays have signal content that can be associated with one of the two patterns. That is, these points correspond to frequencies at which nonoverlapped spectral features are found in the spectra. The scatter of the points about the rays is due to noise. The most distant points from the origin represent the most intense spectral features in a pattern.

**3. Points That Cross between, and Possibly through, Rays.** These points correspond to frequencies at which peaks from two or more patterns overlap.

The points in category 2 are of the greatest interest from the standpoint of identifying patterns in the spectra. The presence of two rays of points in the recursion map clearly indicates that two patterns are present in the data set. The upper of these rays comprises points that are well-described by

$$I_1 \approx a_1 I_A \tag{6}$$

$$I_2 \approx a_2 I_A \tag{7}$$

while the lower ray comprises points well-described by

$$I_1 \approx b_1 I_B \tag{8}$$

$$I_2 \approx b_2 I_B \tag{9}$$

Thus, each pattern can be considered to be defined by sets of points on the recursion map for which the ratio of intensities in the two spectra is nearly constant. This ratio of intensities is referred to as the *ratio direction*, and each pattern contained in the spectra can be uniquely labeled by a ratio direction. In experimental data, however, the ratio directions are not known and it is the task of the XCC to determine an unbiased estimate of the ratio direction for each pattern.

Linear least-squares fitting is not ideal for this task because it is a global optimization technique, meaning that it determines *one* set of model parameters which best describes all of the data. By contrast, for the synthetic data, unbiased estimates are desired for *two* ratio directions. To accomplish this task, we defined our own figure-of-merit function, $G$, which in the case of two data records takes the form

$$G(\alpha) = \sum_k g_k(\alpha) = \sum_k R_k \exp(-d_k^2 / 2\sigma^2) \tag{10}$$

Since the "fit line" is constrained to pass through the origin, the merit function is taken to be a function of just one parameter, $\alpha$, which represents the ratio direction. The sum over $k$ represents a sum over all points on the recursion map. The $g_k$ are referred to as weight functions; thus, the merit function takes the form of a sum of weight functions, which are computed for each point on the recursion map.

The precise form of the XCC merit function is justified in refs 29 and 30. Here we note simply that it is defined as a product of two functions. The first term $R$ is the distance of a point on the recursion map from the origin; it weights more intense points in the spectra more strongly, because these points

are less likely to be corrupted by noise or overlap with other peaks. The second term is a Gaussian function of $d_k$, the distance of a point from the fit line, and thus this term weights points that are close to the fit line more strongly than those far from the fit line ($\sigma$ is the experimental noise). In a technical sense, this term makes the XCC a "redescending robust estimator". "Robust estimators"[32–35] in general are those that are influenced by outliers to a lesser degree than the $\chi^2$ function used in least-squares fitting. *Redescending* robust estimators[32–34] are a special class of robust estimators which, in contrast to least-squares fitting, weight outliers *less* strongly than those points that are well-described by the model. A redescending robust estimator is desirable for the task of identifying the two model ratio directions in the recursion map precisely because extraction of more than one model estimate is desired.

The fourth panel in Figure 3 depicts the XCC merit function as a function of ratio direction (here, the ratio direction is represented by the angle between the fit line and the *x*-axis) for the simulated spectra. Two maxima are observed in the merit function at 20.1° and 47.5°. These values differ only slightly from the values of 18.4° and 48.0° used to construct the synthetic spectra.

With the number of patterns and the ratio directions identified, it is now possible to assign spectral features to patterns. The most straightforward method for doing so is to note that eq 4 is invertible, i.e.,

$$I_a(x) = \frac{1}{a_1 b_2 - a_2 b_1} [b_2 I_1(x) - b_1 I_2(x)] \tag{11}$$

$$I_b(x) = \frac{1}{a_1 b_2 - a_2 b_1} [-a_2 I_1(x) + a_1 I_2(x)] \tag{12}$$

Therefore the pattern intensities at any given frequency can be determined from the spectral intensities if the coefficients $a_1$, $a_2$, $b_1$, and $b_2$ are known. The coefficients $a$ and $b$ are equivalent to the pattern ratio directions determined by XCC. Although it may appear that we are attempting to use two pattern ratio directions to determine four coefficients, any two of the coefficients (such as $a_1$ and $b_1$) can be assigned arbitrary values; this is equivalent to introducing arbitrary scaling factors for the patterns, $I_a$ and $I_b$. The results of this "linear inversion" procedure for the synthetic data set are depicted in the bottom panel of Figure 3. The patterns recovered from the spectra are essentially identical to those used to construct the spectra, although the recovered patterns of course have finite signal-to-noise. Note in particular that the linear inversion succeeds in recovering the line shapes of the two lines that were overlapped in the synthetic spectra.

## IV. Pure Bending Dynamics

Although we have only illustrated the application of the XCC to a pair of spectra, it can be readily generalized to treat an arbitrary number of spectra.[30,31] In the case of the acetylene DF spectra, the XCC was utilized to identify fractionated bright state patterns that are repeated in 5 spectra recorded using different intermediate vibrational states. The results of this procedure for the 14 000–15 000 cm$^{-1}$ region are shown at the bottom of Figure 2. Note in particular that the XCC succeeds in disentangling two heavily overlapped patterns in the 14 500–14 900 cm$^{-1}$ region. The ability to identify these fractionated bright states up to 15 000 cm$^{-1}$ provides substantial evidence that the acetylene polyad numbers remain conserved on a time scale of at least 1 ps up to the threshold of isomerization. In
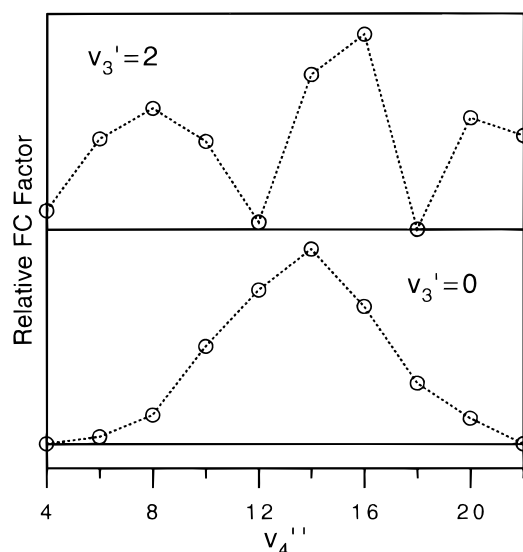
**Figure 4.** Experimentally determined relative Franck–Condon factors for the $(0, 1, 0, \nu_4, 0)$ bright states in the $2\nu_3'$ (top) and origin band (bottom) DF spectra.

fact, fractionated bright states can continue to be identified even above the isomerization barrier, a result that will be discussed in a forthcoming publication.[36]

In addition to the fractionation patterns, the numerical pattern recognition approach also permits the determination of bright state Franck–Condon factors for acetylene at high internal energy. Experimental Franck–Condon factors for highly excited states in polyatomic molecules are generally difficult to obtain due to the interference of IVR, but the pattern recognition analysis identifies all of the vibrational levels that gain their intensity from a single bright state, and thus the fractionation patterns in any given spectrum can simply be integrated to obtain the relative Franck–Condon factor for each of the bright states. A small subset of these Franck–Condon factors is presented in Figure 4, and it is clear that these are consistent with qualitative Franck–Condon arguments. That is, two dips are observed in the trans bend Franck–Condon factors observed in emission from the $2\nu_3'$ vibrational level of the $S_1$ state, while no dips are observed from the vibrationless level (origin band). In terms of quantitative prediction, however, our deperturbed Franck–Condon factors up to 15 000 cm$^{-1}$ provide a substantial challenge for theory. J. K. G. Watson has performed harmonic and anharmonic Franck–Condon calculations for the acetylene $S_1 \rightarrow S_0$ system,[37] with good agreement with experiment for the anharmonic calculations.[93] Two groups of theoreticians[38,39] also plan to perform anharmonic Franck–Condon calculations for acetylene using vibron models, which are algebraic models that can explicitly incorporate mode anharmonicity.

Our interest here, however, is with the insights that can be gained into acetylene vibrational dynamics at high vibrational energy, and the apportioning of the DF spectra into bright state progressions constitutes the crucial first step. The fractionation pattern for each bright state encodes its IVR—the redistribution of the vibrational excitation from the Franck–Condon active modes (CC stretch and trans bend) into the remaining degrees of freedom. Even without any detailed analysis, the bright state fractionation patterns at the bottom of Figure 2 clearly indicate that the rate of IVR at high internal energy is highly sensitive to the way in which vibrational excitation is divided among the two Franck–Condon active modes. Specifically, the two bright states with the greatest excitation in the CC stretch mode, $(0, 5, 0, 8, 0)$ and $(0, 6, 0, 6, 0)$, *display*

*no detectable fractionation*, indicating minimal IVR. That is, there exist vibrational levels near the isomerization barrier (and even above it; see ref 40) that can continue to be labeled with normal mode quantum numbers, despite the fact that the majority of bright states at this energy display quite extensive fractionation (fast IVR). This anomalously slow IVR, which is examined in detail in ref 40, is due largely to the isolation of the bright states in question from other states in the same polyad. That is, these bright states are by far the lowest energy states in their respective polyads, and the nearest states with which they can interact are >100 cm$^{-1}$ higher in energy.

From a dynamical viewpoint, the most interesting fractionation pattern in Figure 2 is that of $(0, 0, 0, 22, 0)$. The trans bend mode is the lowest frequency normal mode in acetylene, and thus this fractionation pattern encodes the largest amplitude motions that can be studied below the isomerization barrier in our DF spectra. This bright state is one member of a long progression of "pure bending" bright states, $(0, 0, 0, \nu_4, 0)$, which involve no excitation in the stretching modes and thus belong to polyads with $N_s = 0$. For this set of polyads, the $N_{res}$ quantum number simplifies to

$$N_{res} = \nu_4 + \nu_5 = N_b$$

in which $N_b$, the number of quanta of bend excitation, is introduced as a shorthand notation for the $N_{res}$ and $N_s$ polyad numbers for the pure bending polyads. Note that, because *all* states in the pure bending polyads have no stretch excitation, the only IVR pathways that are available for the pure trans-bend bright states are those that exchange vibrational energy and angular momentum between the trans and cis bend modes. This does not imply, however, that the IVR is simple. On the contrary, the trans bend bright state fractionation patterns become quite complex as early as ~9000 cm$^{-1}$, as can be seen in Figure 5.

The complexity of the $(0, 0, 0, \nu_4, 0)$ bright state fractionation patterns necessitates the use of a numerical model to gain insight into the mechanism of the IVR. As will be seen below, the complex fractionation patterns encode a simple but profound change in the vibrational dynamics as a function of bend excitation, which is not at all obvious by simply inspecting the patterns. In principle, one could determine from the data a potential energy surface for the ground electronic state. That is, one could define an appropriate analytical expression to represent the potential energy surface, and adjust the parameters to achieve maximal agreement between the observed eigenenergies and those calculated using the surface. However, six vibrational degree of freedom systems at high vibrational energy currently represent the state of the art in fully quantum mechanical, variational calculations (such calculations have only recently become routine for triatomic molecules at high vibrational excitation; see for example refs 41 and 42), Thus, our results present a challenge for both electronic and vibrational structure calculations (i.e., can a potential energy surface be constructed that reproduces our results, at least qualitatively, to 15 000 cm$^{-1}$, and can fully 6D variational[43,44] or wave packet propagation[45] methods be used efficiently to investigate the spectra and dynamics of acetylene at high internal energy?). It should be noted that some work has been done to develop potential energy surfaces[46,47] and force fields[43,48] for $S_0$ acetylene and vinylidene, and in some cases these potentials have been refined against (certain) experimental data. However, no representation of the $S_0$ potential energy surface has yet been

Feature Article

*J. Phys. Chem. A, Vol. 104, No. 14, 2000* **3079**
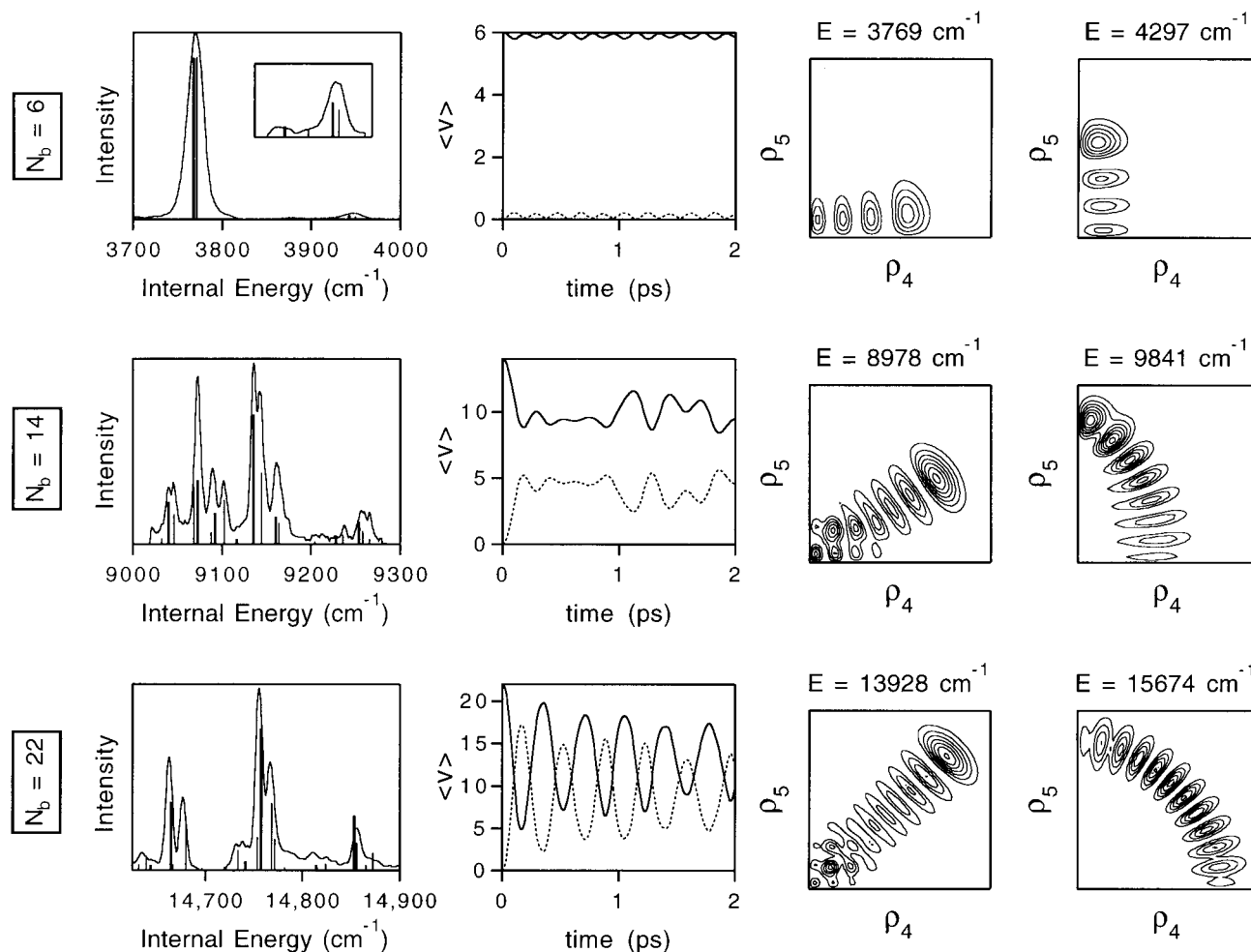


**Figure 5.** First column: Comparison of experimental results and the effective Hamiltonian model. The solid lines represent the fractionation patterns for the (0, 0, 0, 6, 0), (0, 0, 0, 14, 0), (0, 0, 0, 22, 0) bright states that were extracted from the DF data set using XCC. The inset in the upper left part provides a close-up view of the (0, 0, 0, 6, 0) fractionation pattern above 3850 cm$^{-1}$. The vertical sticks (thick for $l = 0$, thin for $l = 2$) represent the eigenstate energies and relative intensities predicted by the $H^{\text{eff}}$. Second column: Hypothetical time domain evolution of the $l = 0$ bright state wave packets as predicted by the and as represented by the $H^{\text{eff}}$ average number of quanta in the trans (solid line) and cis (dotted line) bend modes. Third and fourth columns: The lowest and highest energy eigenstates in each $l = 0$ polyad, projected onto the ($\rho_4, \rho_5$) plane.

demonstrated to reproduce the highly excited bending states near 15 000 cm$^{-1}$ that are the central concern in the remainder of this article.

In the absence of a potential surface with sufficient accuracy, which becomes increasingly problematic for larger molecules, effective Hamiltonian models can provide substantial insights into quantum vibrational dynamics. In fact, even when accurate potential energy surfaces are available, effective Hamiltonian models (which can be derived from the potential by perturbation theory[47,49]) are still frequently found to provide insights that are complementary to calculations performed directly from a potential surface; see, for example, recent work on acetylene by Sibert and McCoy[47,50] and a series of recent papers on HCP,[42,49,51−53] which together represent an experimental and theoretical *tour de force* and provide excellent examples of the complementarity of effective Hamiltonians and potential surfaces for spectrum interpretation. For the purposes of this article, an effective Hamiltonian will be defined as a Hamiltonian that can be written entirely in terms of the (harmonic) raising and lowering operators for the various vibrational degrees of freedom of the molecule, which are often chosen to be the normal modes of vibration, although other choices are possible (see refs 54 and 55 for examples of local mode models applied to the acetylene bend degrees of freedom). Each of the bend normal modes for acetylene, trans and cis, are doubly degenerate,

and thus the bending effective Hamiltonian is expressed in terms of raising and lowering operators for the two-dimensional (2D) harmonic oscillator. These operators are labeled d (right) and g (left), using the notation of Cohen-Tannoudji et al.[56] and are defined as

$$\hat{a}_{\text{d}} = \frac{1}{\sqrt{2}}(\hat{a}_x - i\hat{a}_y) \tag{13}$$

$$\hat{a}_{\text{g}} = \frac{1}{\sqrt{2}}(\hat{a}_x + i\hat{a}_y) \tag{14}$$

where $x/y$ represent the two equivalent rectilinear coordinates for the 2D oscillator. The $d/g$ operators have the convenient property that the number operators corresponding to the conventional quantum number labels for the 2D oscillator can be expressed as

$$\hat{v} = \hat{v}_d + \hat{v}_g = \hat{a}_d^\dagger \hat{a}_d + \hat{a}_g^\dagger \hat{a}_g \tag{15}$$

$$\hat{l} = \hat{v}_d - \hat{v}_g = \hat{a}_d^\dagger \hat{a}_d - \hat{a}_g^\dagger \hat{a}_g \tag{16}$$

Using the conventional "4" and "5" labels for trans and cis, respectively, the bending effective Hamiltonian is defined as

$$\hat{H}^{\text{eff}} = \omega_4 \hat{v}_4 + \omega_5 \hat{v}_5$$

$$+ x_{44}\hat{v}_4\hat{v}_4 + x_{45}\hat{v}_4\hat{v}_5 + x_{55}\hat{v}_5\hat{v}_5$$

$$+ y_{444}\hat{v}_4\hat{v}_4\hat{v}_4 + y_{445}\hat{v}_4\hat{v}_4\hat{v}_5 + y_{455}\hat{v}_4\hat{v}_5\hat{v}_5 + y_{555}\hat{v}_5\hat{v}_5\hat{v}_5$$

$$+ g_{44}\hat{l}_4\hat{l}_4 + g_{45}\hat{l}_4\hat{l}_5 + g_{55}\hat{l}_5\hat{l}_5$$

$$+ s_{45}(\hat{a}_{4d}^\dagger \hat{a}_{4g}^\dagger \hat{a}_{5d}\hat{a}_{5g} + \hat{a}_{4d}\hat{a}_{4g}\hat{a}_{5d}^\dagger \hat{a}_{5g}^\dagger)$$

$$+ [r_{45}^\circ + r_{445}(\hat{v}_4 - 1) + r_{545}(\hat{v}_5 - 1)](\hat{a}_{4d}\hat{a}_{4g}^\dagger \hat{a}_{5d}^\dagger \hat{a}_{5g} +$$
$$\hat{a}_{4d}^\dagger \hat{a}_{4g}\hat{a}_{5d}\hat{a}_{5g}^\dagger)$$

$$+ \frac{1}{4}[r_{45}^\circ + r_{445}(\hat{v}_4 - 1) + r_{545}(\hat{v}_5 - 1) +$$
$$2g_{45}](\hat{a}_{4d}^\dagger \hat{a}_{4d}^\dagger \hat{a}_{5d}\hat{a}_{5d} + \hat{a}_{4g}^\dagger \hat{a}_{4g}^\dagger \hat{a}_{5g}\hat{a}_{5g} + \hat{a}_{4d}\hat{a}_{4d}\hat{a}_{5d}^\dagger \hat{a}_{5d}^\dagger +$$
$$\hat{a}_{4g}\hat{a}_{4g}\hat{a}_{5g}^\dagger \hat{a}_{5g}^\dagger) \quad (17)$$

Although this expression for the $H^{\text{eff}}$ may look complicated, it simply encodes harmonic oscillator scaling rules for the anharmonic couplings between the normal mode states. Specifically, the $\omega$ terms are the harmonic contributions, the $x$, $y$, and $g$ terms represent diagonal anharmonicities, and the remaining terms, parametrized by $r_{45}$ and $s_{45}$, are the off-diagonal anharmonic resonances (Darling-Dennison and vibrational $l$-resonance). It should be noted that this Hamiltonian is quite similar in form to older models of Plíva[57] and Herman;[10] the major contribution of our model is that our fitted parameters reproduce the experimental data to much higher energy.

The parameters in this model were fitted to a set of 83 vibrational energy levels, 51 of which were derived from our DF data set and the remainder of which were derived from previously published absorption data (the absorption data include vibrational levels with at most four quanta of bend excitation). The inclusion of the high energy DF data presented a number of challenges for the fit, the most serious of which was establishing correspondences between the calculated and observed vibrational energy levels. That is, at high energy, only a small fraction of the eigenstates within a given polyad are observable within the signal-to-noise of the experiment, and the fitting routine must decide in an automated fashion which calculated eigenstate corresponds to which observed transition in order to calculate the ($\chi^2$) merit function. Our solution to this challenge and others are detailed in ref 58. The final set of 16 fitted parameters, which is listed in Table 2 of ref 58, reproduces the 83 vibrational energy levels up to 15 000 cm$^{-1}$ with an RMS accuracy of 1.4 cm$^{-1}$. The agreement between the model and the experimental data is depicted in the left column of Figure 5 for 3 specific bright states. Here it can be seen that the relative intensities predicted by the $H^{\text{eff}}$ (from the character of the bright state in each eigenstate) also agree well with experiment, although intensities were not included in the fit. Note also that the final fitted model makes it possible to partition the bright state fractionation patterns into their $l = 0$ and 2 components.

It is worth reiterating that the development of an $H^{\text{eff}}$ with predictive power for the very large amplitude bends is possible only because single fractionated bright states can be extracted from the DF data set using numerical pattern recognition, despite severe, systematic overlap between many fractionated bright state patterns. Having developed a numerical model with excellent predictive power, we now turn to the insights that this model permits into vibrational energy flow. We have already stated that the bright state fractionation patterns encode the IVR; for instance, the width of a fractionation pattern provides a direct

measure of the rate of vibrational energy transfer out of the bright state. However, the effective Hamiltonian model permits us to ask much more detailed questions about the vibrational energy flow, such as to where does the energy flow, and by what mechanism? Please note that although both $l = 0$ and $l = 2$ states are observed experimentally, the discussion below will focus exclusively on the $l = 0$ states.

The starting point for studying the vibrational energy flow is the time evolution of the zero-order bright state, which is nonstationary since it is not an eigenstate:

$$\Psi(t) = \sum_{j=1}^{N} c_j \psi_j e^{-i\omega_j t} \quad (18)$$

in which $\psi_j$ are the eigenstates, $\omega_j$ are the corresponding frequencies ($E_j/h$), $\Psi(0)$ is the bright state, $c_j = \langle \Psi(0)|\psi_j\rangle$, and $N$ is the number of states within the relevant polyad. The coefficients $c_j$ are known from the unitary transformation that diagonalizes the $H^{\text{eff}}$, and thus *the time-evolution of the initially prepared bright state is completely determined from information obtainable from the frequency domain spectrum.*

The survival probability of the initially prepared state $|\langle \Psi(0)|\Psi(t)\rangle|^2$ is frequently used to represent this dynamics. The survival probability does not, however, provide a complete picture of the dynamics, in the sense that when the survival probability is low, the overlap of the wave packet with other zero-order states must be relatively large—but which zero-order states? One could, of course, calculate the overlap of the time-evolving wave packet with any of the zero-order states in the relevant polyad, but for the ($N_b = 22$, $l = 0$) polyad, for example, the total number of zero-order states is 42, and it is not practical to plot the overlap of the wave packet with *each* of these states. A useful overview of the time-domain dynamics is provided by the time evolution of the expectation values of the number operators $\hat{v}_4$ and $\hat{v}_4$:

$$\langle v_b(t)\rangle = \langle \Psi(t)|\hat{v}_b|\Psi(t)\rangle \quad (19)$$

In colloquial terms, $\langle v_4(t)\rangle$ and $\langle v_5(t)\rangle$ represent the time-dependent average number of quanta in the trans and cis bend modes, respectively, and these measures are plotted in the second column of Figure 5 for the wave packets corresponding to the initially prepared (0, 0, 0, 6°, 0°), (0, 0, 0, 14°, 0°), and (0, 0, 0, 22°, 0°) bright states. Note that $\langle v_4(0)\rangle = N_b$, $\langle v_5(0)\rangle = 0$, and that $\langle v_4(t)\rangle + \langle v_5(t)\rangle = N_b$ at all times.

These expectation values make it clear that the IVR associated with the (0, 0, 0, 6°, 0°) bright state is quite minimal, in the sense that very little energy is exchanged between trans and cis bend. The minimal IVR reflects the fact that the bright state is *nearly* an eigenstate of the (effective) Hamiltonian; that is, the anharmonicities in the potential surface couple this bright state only minimally to other normal mode states. This fact is clearly observed in the fractionation pattern for the bright state, which consists of one main peak (the nominal bright state), which carries 97.2% of the bright state character, and a much less intense series of peaks located on the high energy side of the main peak, which can be considered "perturbers" of the bright state.

The (0, 0, 0, 14°, 0°) bright state, on the other hand, is not even approximately an eigenstate of the $H^{\text{eff}}$. In the frequency domain, the bright state character is distributed in a complicated manner over many vibrational levels, and the most intense peak in this case accounts for only 38.4% of the bright state character. In the time domain, a substantial fraction of the initial

Feature Article

*J. Phys. Chem. A, Vol. 104, No. 14, 2000* **3081**

excitation in the trans bend mode is rapidly (<200 fs) redistributed to the cis bend mode, and at longer times the vibrational energy is apportioned in a roughly 70%/30% ratio between the trans and cis bend modes, although the energy continues to flow between the two modes in a seemingly random fashion.

For the (0, 0, 0, 22°, 0°) bright state, the extent of the energy flow between the two bend modes is even more extreme, which is expected given that the strength of the anharmonic couplings should continue to grow with increasing energy. However, the energy flow between trans and cis is also unexpectedly regular. In only 170 fs, nearly 80% of the vibrational excitation has flowed from trans bend into cis bend, but then just as quickly, nearly all of it flows right back to trans bend. These regular oscillations continue for several picoseconds. A close look at the fractionation pattern for (0, 0, 0, 22°, 0°) reveals a surprising regularity as well (as it must, since the frequency and time domain representations of IVR are equivalent). The $l = 0$ pattern consists primarily of just 3 lines, which are spaced at intervals of $\sim$95 cm$^{-1}$; these three eigenstates account for 72.0% of the bright state character, and the most intense peak accounts for 43.3%.

Taken together, the plots in the two left columns of Figure 5 indicate that the complexity of IVR for the trans bending bright states is not a simple function of internal energy. In particular, the dynamics in the $N_b = 22$ polyad seems mysterious, being both extensive (strong exchange of energy between trans and cis) and simple (regular recurrences). The physical basis for this behavior is considered in the next section.

## V. Local Mode Behavior

In the preceding section, we considered vibrational energy flow in the acetylene bend system from a *basis set dependent* point of view. Specifically, we monitored the wave packet evolution of three trans bend bright states in terms of vibrational energy flow among the normal modes. The particular bright states were chosen because they were experimentally observed and because they are representative of the major changes in dynamics as a function of vibrational energy. However, the trans bend bright states are only one class of an infinite number of wave packets that one could imagine propagating using the effective Hamiltonian. One could, for instance, investigate pure cis bend bright states, (0, 0, 0, 0, $\nu_5$). Although these "hypothetical" bright states have not been observed experimentally, the $H^{eff}$ could be used to predict their IVR. One could even choose classes of bright states that do not involve the normal mode motions at all, such as a hypothetical "local bend" bright state, which would involve bend excitation in a single bond. The IVR associated with each different hypothetical bright state provides a different viewpoint on the vibrational energy flow at a given energy, but no single one by itself provides a complete picture.

To gain a more complete understanding of the vibrational energy flow as a function of energy, one can ask basis set *independent* questions about the vibrational structure, such as "what are the stable vibrational modes at any given energy?" More precisely, do there exist any vibrational modes (which can be unrelated to the normal modes) of the molecule into which energy can be placed with minimal subsequent vibrational energy redistribution? As can be seen in the top row of Figure 5, the normal mode bending motions are stable at sufficiently low internal energy because little energy is exchanged between trans and cis bend. At $N_b = 22$, the normal mode motions are highly unstable by the same definition, but the regular oscillations associated with the vibrational energy flow suggest that

the large-amplitude bending dynamics are unlikely to be highly "chaotic" and that there might therefore exist stable (nonnormal mode) vibrational motions at high energy.

In this section, two approaches to the question of regularity vs chaos at high energy will be employed: visual examination of the eigenfunctions of the $H_{eff}$, and nonlinear classical mechanics, the former of which will be considered first. The $H^{eff}$ is evaluated, of course, in a product basis set of two 2D harmonic oscillators, which represent the trans and cis bend degrees of freedom. The eigenvector matrix that results from diagonalization of the $H^{eff}$ permits any eigenfunction to be expressed as a linear superposition of the zero-order basis states. Thus, the most natural coordinates for graphical representation of the eigenvectors are ($\rho_4$, $\phi_4$, $\rho_5$, $\phi_5$), where $\rho$ and $\phi$ are the radial and angular coordinates for the 2D isotropic harmonic oscillator, the wave functions of which take the form

$$\Psi_{\nu,l}(\rho,\phi) = \chi_\nu^{|l|}(\rho)e^{il\phi} \qquad (20)$$

$$\chi_\nu^{|l|}(\rho) = N_{\nu,|l|}e^{-\rho^2/2}\rho^{|l|}L_{(\nu+l)/2}^{|l|}(\rho^2) \qquad (21)$$

$L$ represents the associated Laguerre polynomials, and $N$ is a normalization constant. All eigenfunction plots considered below represent projections of the probability density onto the ($\rho_4$,$\rho_5$) plane; for discussion of the angular dependence of the wave functions, see ref 54.

The third and fourth columns of Figure 5 represent the lowest and highest energy eigenstates within the $N_b = 6$, 14, and 22 polyads. In the $N_b = 6$ polyad, both eigenfunctions can clearly be assigned normal mode quantum numbers. In the case of the lowest energy eigenfunction, there is a single nodal coordinate that runs nearly parallel to the trans bend axis. This state is the nominal bright state for the polyad, (0, 0, 0, 6°, 0°); as discussed in the preceding section, this eigenstate carries 97.2% of the bright state character. Note that, in terms of counting nodes in these plots, it should be kept in mind that the radial coordinates only take positive values. Thus, the number of nodes (except those at the domain boundaries) should be doubled. The highest energy eigenstate in the polyad is equally easy to assign as (0, 0, 0, 0°, 6°).

The eigenfunctions at high energy, $N_b = 22$, are profoundly different. Although both of the eigenfunctions shown in Figure 5 have well-defined nodal coordinates, in neither case do they run parallel to the axes, which implies that there exist stable vibrational motions at high internal energy that are unrelated to the normal mode motions. The lowest energy eigenstate in the polyad (third column) is easier to interpret. For this eigenstate, there is a single nodal coordinate which runs along $\rho_4 = \rho_5$. Classically, the simultaneous excitation of the trans and cis bending motions with the same amplitude leads to the bending of just one hydrogen, and thus this eigenstate is associated with a *local bending* motion, which has also been reported in other classical, semiclassical, and quantum studies of acetylene.[50,59−61]

The highest energy eigenstate in the polyad is more difficult to interpret in this set of coordinates. The nodes of this eigenfunction align along a coordinate defined by $\rho_4^2 + \rho_5^2 \approx C$, where $C$ is a constant. The absence of substantial probability near ($\rho_4 = 0$, $\rho_5 = 0$) implies that the vibrational motion never passes through the linear configuration. On the other hand, the motion must pass through the trans and cis planar configurations, due to the lobes of probability located near $\rho_4 = 0$ (with nonzero displacement in $\rho_5$) and $\rho_5 = 0$ (with nonzero displacement in $\rho_4$). A careful consideration of this eigenstate (see ref 54) reveals
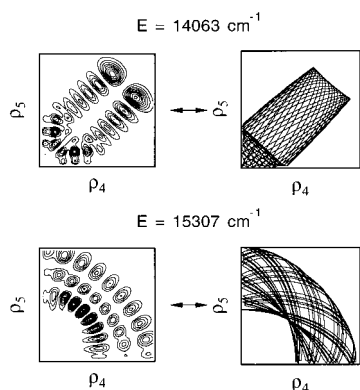
**Figure 6.** Quantum-classical correspondence. The periodic orbits (right) are isoenergetic with the eigenfunctions (left) and plotted in the same coordinates.

that it corresponds to a molecular motion in which the two hydrogens maintain a given angle with respect to the CC axis, but execute an internal rotation that changes the torsional angle between them. Since total vibrational angular momentum must be conserved, the two hydrogens execute rotations in the opposite sense, and this eigenstate is identified with a "counter-rotating" motion. To our knowledge, the counter-rotation motion has not been reported in previous studies.

Obviously, the two eigenstates displayed in Figure 5 represent a small fraction of the eigenstates in the $N_b = 22$ polyad. Among the eigenfunctions that are not depicted, there are a few that are quite complicated and are not easily assignable to any simple bending motion, but the majority of bending eigenstates at high energy can be classified as either local bend or counter-rotation (none are clearly assignable as normal mode states). Two other $N_b = 22$ eigenstates are shown in the left column of Figure 6. The upper of the two is representative of many eigenstates near the bottom of the polyad that appear to be quite similar to the pure local bend state in Figure 5 but have a more complicated nodal structure (here, there is a second nodal coordinate orthogonal to $\rho_4 = \rho_5$). The lower eigenstate in Figure 6 is representative of many eigenstates near the top of the polyad that are closely related to the pure counter-rotation state in Figure 5. As discussed in some detail in ref 54, the precise assignments of these "imperfect" local bend and counter-rotation states can be resolved by transforming the eigenfunctions, and the effective Hamiltonian, to a new set of *local mode* coordinates that are defined as positive and negative superpositions of the normal mode coordinates. In the local mode basis set, it becomes clear that states such as those in Figure 6 represent motions intermediate between local bend and counter-rotation.

In the preceding discussion, we have associated classical motions with quantum eigenstates, based largely upon the strong localization of probability around clearly defined nodal coordinates in the wave functions that we considered. However, the issue of quantum-classical correspondence can also be studied explicitly for this system, by transforming the quantum effective Hamiltonian to a classical one, using standard semiclassical rules (i.e., by using the substitution[62] $\hat{a}_j \rightarrow I_j \exp(-i\phi_j)$ in eq 17). We have done so, and in collaboration with Profs. Howard S. Taylor (USC) and Christof Jung (UNAM), have performed (nonlinear) classical mechanical calculations on the system to investigate the structure of the classical phase space.[63] [It should be noted that several other classical and semiclassical studies of acetylene have been performed, including the early work of Holme and Levine,[64−66] the Farantos et al.[67] study using the Halonen, Child, and Carter surface,[46] and studies by Kellman,[59,68] McCoy and Sibert,[50] and van der Pals and Gaspard.[61]
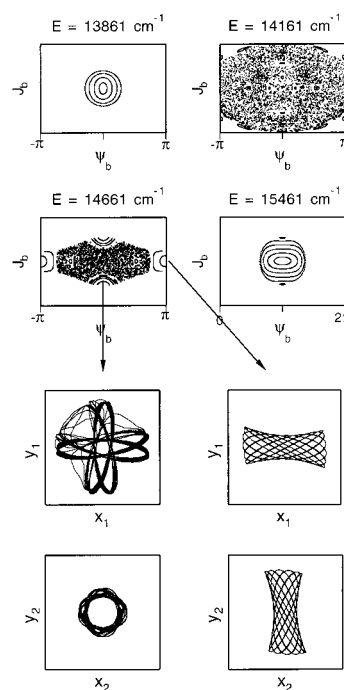


**Figure 7.** Overview of the classical dynamics associated with the ($N_b = 22, l = 0$) polyad. Top two rows: Surfaces of section at four different energies within the polyad. Bottom two rows: Two stable periodic orbit motions that coexist with chaos in the middle of the polyad. Both of these motions can be considered compromises between the local bend and counter-rotation motions that dominate at the bottom and top of the polyad, respectively.

Our study is the first, however, that is based upon a model that reproduces the bending vibrational levels to very high internal energy (15 000 cm$^{-1}$).]

At low internal energy, the classical mechanical calculations confirm, as expected, the dominance of the normal mode motions. At higher internal energy, however, qualitatively different stable vibrational motions are born, as well as large-scale classical chaos, which can be identified as low in energy as 5200 cm$^{-1}$. Figure 7 provides an overview of the classical dynamics in the ($N_b = 22, l = 0$) polyad, using four surfaces of section (SOS), which represent the intersection of classical trajectories with a particular plane that cuts through phase space. Periodic orbits are fixed points on the surface of section, and when stable are surrounded by concentric circles that represent quasi-periodic trajectories. Chaos, on the other hand, tends to look like a randomly pattern of unrelated points.

The SOSs at 13 861 and 15 461 cm$^{-1}$ are both dominated by regularity and are representative of the classical dynamics near the bottom and top of the $N_b = 22$ polyad, respectively. In the case of the 13 861 cm$^{-1}$ SOS, the periodic orbit at the center of the concentric circles represents a local bend periodic orbit, whereas the organizing periodic orbit motion in the 15 461 cm$^{-1}$ SOS represents the counter-rotation motion. The dominance of regularity at the bottom and top of the polyad explains why the majority of the states at the extremes of the polyad can be assigned in terms of the local bend and counter-rotation motions. Figure 6 presents two specific examples of quantum-classical correspondence. The quasi-periodic trajectories on the right are isoenergetic with the eigenstates on the left and plotted in the same set of coordinates. The correspondence is striking in both cases. Notice especially how the probability in the $E = 15\,307$ cm$^{-1}$ quantum eigenfunction accumulates near regions in configuration space where the periodic orbit passes many times.

At intermediate energies, as represented by the 14 161 and

Feature Article

*J. Phys. Chem. A, Vol. 104, No. 14, 2000* **3083**
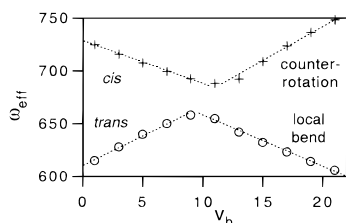


**Figure 8.** Effective frequencies of the normal and local mode motions as a function of energy. $N_b \approx 10$ marks the transition between normal and local mode behavior, with the trans bending motion becoming local bend, and cis bend becoming counter-rotation.

14 661 cm$^{-1}$ surfaces of section, classical chaos plays a role, and at some energies even dominates the phase space. The surface of section at $E = 14\,661$ cm$^{-1}$ demonstrates an intriguing coexistence of stable vibrational motions and chaos. The two most stable periodic orbit motions that can be identified in this SOS are depicted at the bottom of Figure 7. In the periodic motion on the left, one of the two hydrogens undergoes a primarily circular motion, reminiscent of the counter-rotation motion, while the motion of the other is reminiscent of a local bend, although the approximate plane of the bend switches its orientation periodically by $\pi/2$. Due to the conservation of vibrational angular momentum, however, both the "rectilinear" and "circular" motions of the hydrogens are distorted in such a way as to conserve zero total internal angular momentum at all times. The periodic orbit on the right in Figure 7 can also be considered a compromise between the local bend and counter-rotation motions, in the sense that each hydrogen vibrates largely along a plane, but with some superimposed rotation. Several quantum eigenstates can be assigned in terms of these "compromise" motions between local bend and counter-rotation. More surprisingly, however, our detailed study of quantum-classical correspondence in this polyad[63] reveals that, even at energies (such as 14 161 cm$^{-1}$) where classical chaos envelopes nearly the entirety of phase space, the majority of the quantum eigenstates can continue to be assigned in terms of periodic orbit motions that are closely related to the local bend and counter-rotation motions.

At this point, we have established that the large-amplitude bending vibrational dynamics of acetylene is dominated by stable local bend and counter-rotation motions, in contrast to the low energy dynamics, where the normal modes dominate. We now turn briefly to the transition between the low and high energy bending dynamics, the effects of which can be observed quite clearly in the $N_b = 14$ eigenstates in Figure 5. In particular, the lowest energy eigenstate in this polyad (third column) provides a bridge between the trans bend and local bend motions, and the highest energy eigenstate is intermediate between the cis bend and counter-rotation motions. However, the transition between normal and local mode behavior is not as smooth as Figure 5 seems to imply. Figure 8 plots the effective frequencies of the bending motions as a function of polyad number. We define the effective frequencies as

$$\omega_{eff}(N_b) = (E_{N_b+1} - E_{N_b-1})/2 \qquad (22)$$

where $E$ represents the energies of either the lowest or highest energy eigenstates in the pure bending polyads. It is clear on the left-hand side of this plot that the effective frequency for the cis bend motion decreases with increasing vibrational excitation, while that for the trans bend motion increases, which reflects the fact that the trans and cis bend modes have opposite anharmonicities; i.e., $x_{44} > 0$ and $x_{55} < 0$. The rate of change

of the effective frequencies with increasing bend excitation remains roughly constant until $N_b \approx 10$, at which point the effective frequencies abruptly reverse course, signaling a sudden change in the vibrational dynamics. The transition trans from bend to local bend appears to occur at slightly lower bend excitation than the transition from cis bend to counter-rotation, but the simple physical picture that emerges is that when the effective frequencies of the two normal mode motions become nearly commensurate, they become unstable (due to the anharmonic resonances) and give birth to qualitatively new motions. This transition has been considered in detail using classical mechanics; see ref 63.

To conclude this section, we wish to point out that the stable large-amplitude local bend and counter-rotation vibrational motions in acetylene are in many ways analogous to the stable local stretch vibrations that have been reported for many molecules in the limit of high stretch excitation.[69−74] A large body of literature has appeared related to local stretch phenomena, and one of the major achievements of this work was the demonstration that effective Hamiltonian models could be defined for these systems using *either* normal mode or local mode coordinates, and that in fact these alternative representations are formally equivalent.[75−82] In this article, we have considered only the normal mode representation of the acetylene bending dynamics, but this dynamics can be described equally well using a local mode effective Hamiltonian, which can be derived analytically from the normal mode model.[54,83] However, despite these similarities, the local mode behavior in the acetylene bend degrees of freedom, because it involves two *two*-dimensional rather than two *one*-dimensional vibrational modes, encompasses a richer range of motions (such as counter-rotation) for which the conventional language of local stretching systems is not entirely appropriate.

## VI. Conclusion

One recurring theme in our recent work on acetylene has been the contrast between the exceptionally complicated appearance of the experimental spectra and the surprisingly simple vibrational dynamics (either quantum or classical) that can be inferred from these spectra, when properly analyzed. As discussed in section II, much of the *perceived complexity* of acetylene $S_1 \rightarrow S_0$ dispersed fluorescence spectra can be accounted for by the energetic interleaving of polyad fractionation patterns; once these patterns are disentangled from each other, many of the polyad fractionation patterns, which encode the vibrational dynamics of the molecule, are surprisingly simple. A particular surprise was the regularity of the large-amplitude (22 quanta) bending dynamics of acetylene. Although classical chaos does appear to play some role in the high vibrational energy dynamics, the dynamics is nonetheless dominated by a handful of highly stable motions, and thus statistical models of vibrational energy flow are totally inappropriate, at least on a time scale of a few picoseconds.

This conclusion may motivate new strategies for mode selective chemistry. It is possible, for example, to identify pairs of nearly isoenergetic eigenstates that are associated with qualitatively different vibrational motions; such pairs of eigenstates might then be expected to have exploitably distinct chemical properties, such as rates of reaction in certain bimolecular reactions. Our work also presents opportunities for studying vibrational dynamics on the first excited singlet state. The complementary DF and absorption[11] experiments have permitted the acetylene ground vibrational state structure to be sufficiently well characterized that the pattern of emission

(Franck−Condon profile and distribution of intensity within a polyad) from an unassigned $S_1$ vibrational level may help to determine its assignment. Such work is currently underway in the group of Prof. Soji Tsuchiya (Japan Women's University).[23] In a more general sense, we hope that this system will continue to be of interest to experimentalists and theoreticians interested in unimolecular dynamics, because very large amplitude motions of a tetratomic molecule, at chemically significant internal energy, are accurately represented by the model we present.

Having largely succeeded in understanding the short-time, large-amplitude vibrational dynamics of acetylene up to 15 000 cm$^{-1}$, our efforts are now focused on investigating the dynamics at *longer time scales* and *at higher energies*. With respect to longer time scales, SEP spectra with (typically) >0.05 cm$^{-1}$ resolution are capable of probing the dynamics of the molecule on a time scale of <100 ps. An SEP survey spectrum spanning the energy range 4 000−7500 cm$^{-1}$ has been recorded by Prof. David Moss in our laboratory[84] and revealed nearly one-to-one correspondence between the transitions observed in the DF and SEP spectra; in other words, below 7500 cm$^{-1}$, the SEP spectra reveal almost no new dynamics that was not evident from the DF spectra (one weak polyad-breaking Coriolis resonance was observed, but only at $J > 5$). However, as can be seen in Figure 9, at much higher energy (∼ 21 000 cm$^{-1}$), each DF feature corresponds to dozens of SEP transitions. Thus the SEP spectra probe complex dynamical processes on the time scale of tens of picoseconds that are not evident in the DF spectra (this figure presents recent results[85] on $^{13}C_2 H_2$, but the situation in $^{12}C_2 H_2$ will be quite similar). Chaos may play a greater role in this longer time scale dynamics, which is likely to be dominated by higher order resonances, than it does in the lower energy, shorter time scale dynamics considered in this article. However, the ability to assign such complicated SEP spectra recorded at energies well above the isomerization barrier is unlikely to be possible soon. A more productive research direction may be to search systematically for the onsets of longer time scale dynamical processes at energies intermediate between 7500 and 15 000 cm$^{-1}$, by using SEP to probe at higher resolution the features in the DF spectra which have already been assigned to polyads, and can be associated semiclassically with particular types of vibrational motion. Having characterized the first relatively weak and isolated spectroscopic manifestation of a particular resonance (which may or may not conserve the polyad numbers) responsible for a longer time scale dynamical process, then the scaling associated with the resonance will provide testable predictions for the dynamical consequences of the resonance at higher energies.

With respect to the short-time dynamics of acetylene *above* the threshold of isomerization, polyad patterns have been identified as high in energy as 20 000 cm$^{-1}$.[86,87] This does not imply, however, that localized polyad breakdown, and other significant changes in the vibrational structure, do not occur when isomerization first becomes energetically feasible, which is believed to occur at ∼15 200 cm$^{-1}$.[6] The detailed analysis of such changes in the vibrational structure is ongoing, but some qualitative predictions are possible. Specifically, the local bend motions would be expected to play an important role in the near-threshold isomerization dynamics. As illustrated schematically in Figure 1, the transition state for acetylene−vinylidene isomerization is predicted to have a half-linear structure (as predicted by high-level ab initio calculations[3]), in which one CCH angle is ∼60°, while the other is ∼180°. Thus, the minimum energy isomerization coordinate, from linear acetylene
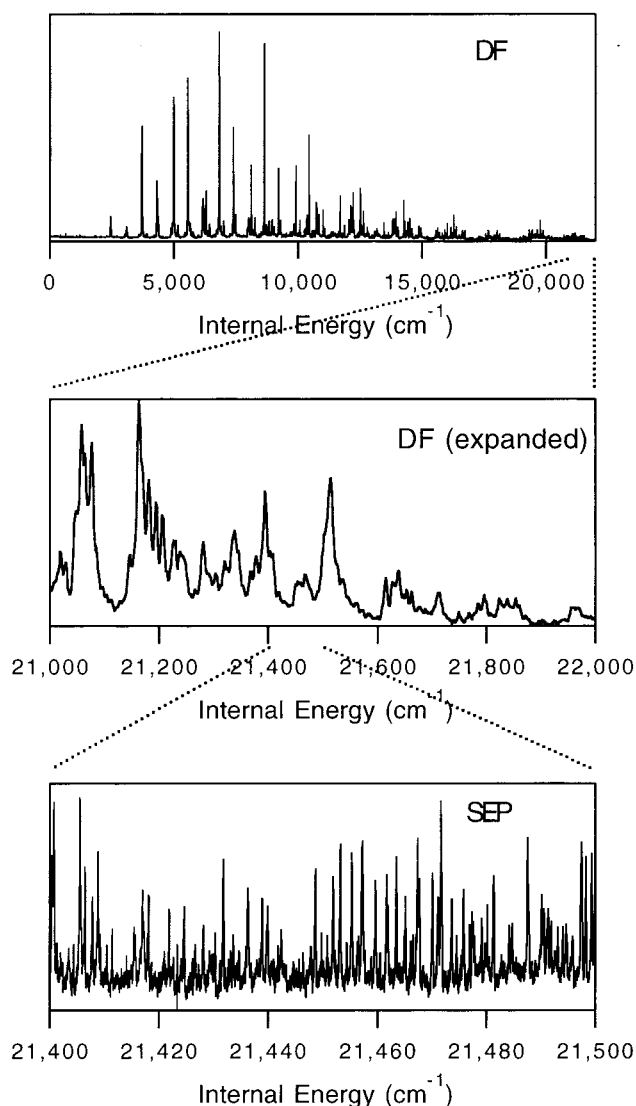


**Figure 9.** Complementary use of DF and SEP spectroscopy to study acetylene dynamics. The spectra in each case are recorded using the $Q(1)$ line of the $2\nu_3'$ band of $^{13}C_2H_2$. Top and middle: DF spectrum (∼16 cm$^{-1}$ resolution). Bottom: SEP spectrum (∼0.15 cm$^{-1}$ resolution).

to the transition state, can be described to a good approximation as a local bend motion.

This observation may help to provide an explanation for some intriguing recent experimental results by the group of Prof. Z. Vager (Weizmann Institute), who performed Coulomb explosion imaging experiments (CEI) on $S_0$ vinylidene, which was prepared by electron photodetachment of the vinylidene negative ion ($H_2CC^-$).[88] The vinylidene rovibrational states that are populated in such an experiment are not eigenstates of the full $S_0$ state Hamiltonian; the vinylidene local minimum is shallow, and tunneling interactions between acetylene and vinylidene are expected to be substantial even for the vibrationless level of vinylidene.[2,5] Thus, the preparation of nominally vinylidene vibrational levels will lead to wave packet dynamics that sample both the vinylidene and linear acetylene wells. Based upon the much larger density of linear acetylene than vinylidene vibrational levels at the same energy, one might expect the vinylidene character to be highly fractionated among many linear acetylene states (i.e., to fall within the "strong coupling" limit[89]); in the time domain, this would correspond to rapid and irreversible isomerization from vinylidene to acetylene.

In the Vager et al. experiments, the molecular structure associated with the evolving wave packet was probed by CEI

Feature Article

*J. Phys. Chem. A, Vol. 104, No. 14, 2000* **3085**

3.5 $\mu$s after the photodissociation of the vinylidene anion. If the isomerization from vinylidene to acetylene were in fact rapid and irreversible, a negligible fraction of the probed molecules would be found in a configuration similar to vinylidene. However, the CEI experiments indicated that ~50% of the molecules could be classified as having structures more similar to vinylidene than to linear acetylene. From this observation, Vager et al. concluded that the vinylidene character of the zero-order states populated in the electron photodetachment experiment are distributed, on average, over 2−3 eigenstates of the $S_0$ surface.

The Vager et al. results are quite surprising, but if their interpretation is proven to be correct, then they may be at least partially explained by the conclusion of our work that the vibrational structure of acetylene near 15 000 cm$^{-1}$ does not even remotely approach the statistical/chaotic limit, even for the low frequency bending modes, and that a handful of stable large-amplitude vibrational motions dominate the dynamics. Specifically, the 2−3 states of linear acetylene into which the vinylidene states are strongly and selectively coupled would almost certainly have a large degree of highly excited local bending character. Because the energy of the vinylidene zero-point level (with respect to the acetylene zero-point level) is not precisely established, it is not possible at this time to identify precisely which acetylene local bending states might be coupled to vinylidene, but it is clear that at any energy near the isomerization transition state, the density of such states is quite small compared with the total density of vibrational states. Theoretical studies of acetylene-vinylidene isomerization[2,90,91] will be critical in establishing more rigorously the connections between the work reported here and the Vager et al. experiments. We wish to point out that previous semiclassical calculations on vinylidene-acetylene isomerization,[2] which predict the decay of vinylidene on a time scale of, at most, several picoseconds, are not necessarily antithetical to the Vager et al. results. The semiclassical calculations investigate the early-time decay of the vinylidene wave packet, which may be quite fast, even if the vinylidene character is distributed over only 2−3 eigenstates. The fast early-time decay, however, would have to be followed by a series of strong and regular partial recurrences (similar to those depicted in the bottom row, second column of Figure 5, although the recurrences would necessarily continue over a much longer time scale than that which is displayed in the figure).

## References and Notes

(1) Osamura, Y.; Schaefer, H. F., III.; Gray, S. K.; Miller, W. H. *J. Am. Chem. Soc.* **1981**, *103*, 1904.

(2) Carrington, T., Jr.; Hubbard, L. M.; Schaefer, H. F., III.; Miller, W. H. *J. Chem. Phys.* **1984**, *80*, 4347.

(3) Gallo, M. M.; Hamilton, T. P.; Schaefer, H. F., III *J. Am. Chem. Soc.* **1990**, *112*, 8714.

(4) Chen, Y.; Jonas, D. M.; Kinsey, J. L.; Field, R. W. *J. Chem. Phys.* **1989**, *91*, 3976.

(5) Ervin, K. M.; Ho, J.; Lineberger, W. C. *J. Chem. Phys.* **1989**, *91*, 5974.

(6) Stanton, J. F.; Gauss, J. *J. Chem. Phys.* **1999**, *110*, 1831.

(7) Yamanouchi, K.; Ikeda, N.; Tsuchiya, S.; Jonas, D. M.; Lundberg, J. K.; Adamson, G. W.; Field, R. W. *J. Chem. Phys.* **1991**, *95*, 6330.

(8) Yamanouchi, K. Private communication.

(9) Abbouti Temsamani, M.; Herman, M. *J. Chem. Phys.* **1995**, *102*, 6371.

(10) Abbouti Temsamani, M.; Herman, M.; Solina, S. A. B.; O'Brien, J. P.; Field, R. W. *J. Chem. Phys.* **1996**, *105*, 11357.

(11) El Idrissi, M. I.; Liévin, J.; Campargue, A.; Herman, M. *J. Chem. Phys.* **1999**, *110*, 2074.

(12) Gutzwiller, M. C. *Chaos in Classical and Quantum Mechanics*; Springer-Verlag: New York, 1990.

(13) Field, R. W.; Coy, S. L.; Solina, S. A. B. *Prog. Theor. Phys.* **1994**, *116*, 143.

(14) O'Brien, J. P. Ph.D. Thesis, Massachussets Institute of Technology, Cambridge, MA, 1997.

(15) Solina, S. A. B. Ph.D. Thesis, Massachussets Institute of Technology, Cambridge, MA, 1996.

(16) Jonas, D. M. Ph.D. Thesis, Massachussets Institute of Technology, Cambridge, MA, 1992.

(17) Chen, Y. Ph.D. Thesis, Massachussets Institute of Technology, Cambridge, MA, 1988.

(18) Abramson, E. H. Ph.D. Thesis, Massachussets Institute of Technology, Cambridge, MA, 1985.

(19) Kittrell, C. In *Molecular Dynamics and Spectroscopy by Stimulated Emission Pumping*; Dai, H.-L., Field, R. W., Eds.; World Scientific: Singapore, 1995; p 109.

(20) Solina, S. A. B.; O'Brien, J. P.; Field, R. W.; Polik, W. F. *J. Chem. Phys.* **1996**, *100*, 7797.

(21) O'Brien, J. P.; Jacobson, M. P.; Sokol, J. J.; Coy, S. L.; Field, R. W. *J. Chem. Phys.* **1998**, *108*, 7100.

(22) Jacobson, M. P. Ph.D. Thesis, Massachussets Institute of Technology, Cambridge, MA, 1999.

(23) Tsuchiya, S. Private communication.

(24) Jonas, D. M.; Solina, S. A. B.; Rajaram, B.; Silbey, R. J.; Field, R. W.; Yamanouchi, K.; Tsuchiya, S. *J. Chem. Phys.* **1993**, *99*, 7350.

(25) Fried, L. E.; Ezra, G. S. *J. Chem. Phys.* **1987**, *86*, 6270.

(26) Kellman, M. E. *J. Chem. Phys.* **1990**, *93*, 6630.

(27) Kellman, M. E.; Chen, G. *J. Chem. Phys.* **1991**, *95*, 8671.

(28) Jaffe, C.; Kellman, M. E. *J. Chem. Phys.* **1990**, *92*, 7196.

(29) Jacobson, M. P.; Coy, S. L.; Field, R. W. *J. Chem. Phys.* **1997**, *107*, 8349.

(30) Coy, S. L.; Jacobson, M. P.; Field, R. W. *J. Chem. Phys.* **1997**, *107*, 8357.

(31) Jacobson, M. P.; Coy, S. L.; Field, R. W.; Lipson, S. J.; Lockwood, R. B.; Vititoe, D. L.; Blumberg, W. A. M.; Armstrong, P. S. *J. Phys. Chem.* submitted.

(32) Ruckstuhl, A. F.; Stahel, W. A.; Dressler, K. *J. Mol. Spectrosc.* **1993**, *160*, 434.

(33) Stahel, W. A.; Ruckstuhl, A. F.; Senn, P.; Dressler, K. *J. Am. Stat. Assoc.* **1994**, *89*, 788.

(34) Ruckstuhl, A. F.; Dressler, K. *J. Mol. Spectrosc.* **1994**, *168*, 185.

(35) Dabrowski, I.; Tokaryk, D. W.; Watson, J. K. G. *J. Mol. Spectrosc.* **1998**, *189*, 95.

(36) Jacobson, M. P.; Silva, M. S.; Duan, Z.-C.; Field, R. W. In preparation.

(37) Watson, J. K. G. In preparation.

(38) Oss, S. Private communication.

(39) Frank, A. Private communication.

(40) Jacobson, M. P.; O'Brien, J. P.; Field, R. W. *J. Chem. Phys.* **1998**, *109*, 3831.

(41) Polyansky, O. L.; Zobov, N. F.; Viti, S.; Tennyson, J.; Bernath, P. F.; Wallace, L. *Science* **1997**, *277*, 346.

(42) Beck, C.; Keller, H.-M.; Grebenshchikov, S. Yu.; Schinke, R.; Farantos, S.; Yamashita, K.; Morokuma, K. *J. Chem. Phys.* **1997**, *107*, 9818.

(43) Bramley, M. J.; Carter, S.; Handy, N. C.; Mills, I. M. *J. Mol. Spectrosc.* **1993**, *157*, 301.

(44) Bentley, J. A.; Wyatt, R. E.; Menou, M.; Leforestier, C. *J. Chem. Phys.* **1992**, *97*, 4255.

(45) Liu, L.; Muckerman, J. T. *J. Chem. Phys.* **1997**, *107*, 3402.

(46) Halonen, L.; Child, M. S.; Carter, S. *Mol. Phys.* **1982**, *47*, 1097.

(47) McCoy, A. B.; Sibert, E. L., III *J. Chem. Phys.* **1996**, *105*, 459.

(48) Martin, J. M. L.; Lee, T. J.; Taylor, P. R. *J. Chem. Phys.* **1998**, *108*, 676.

(49) Joyeux, M. *J. Chem. Phys.* **1998**, *109*, 2111.

(50) Sibert, E. L., III; McCoy, A. B. *J. Chem. Phys.* **1996**, *105*, 469.

(51) Ishikawa, H.; Chen, Y.-T.; Ohshima, Y.; Wang, J.; Field, R. W. *J. Chem. Phys.* **1996**, *105*, 7383.

(52) Ishikawa, H.; Nagao, C.; Mikami, N.; Field, R. W. *J. Chem. Phys.* **1998**, *109*, 492.

(53) Joyeux, M.; Grebenshchikov, S. Yu.; Schinke, R. *J. Chem. Phys.* **1998**, *109*, 8342.

(54) Jacobson, M. P.; Silbey, R. J.; Field, R. W. *J. Chem. Phys.* **1999**, *110*, 845.

(55) Iachello, F.; Oss, S. *J. Chem. Phys.* **1996**, *104*, 6956.

(56) Cohen-Tannoudji, C.; Diu, B.; Laloë, F. *Quantum Mechanics*; Wiley: New York, 1977; Vol. 1, pp 727−741.

(57) Plíva, J. *J. Mol. Spectrosc.* **1982**, *44*, 165.

(58) Jacobson, M. P.; O'Brien, J. P.; Silbey, R. J.; Field, R. W. *J. Chem. Phys.* **1998**, *109*, 121.

(59) Rose, J. P.; Kellman, M. E. *J. Chem. Phys.* **1996**, *105*, 10743.

(60) Sibert, E. L., III; Mayrhofer, R. C. *J. Chem. Phys.* **1993**, *99*, 937.

(61) van Ede van der Pals, P.; Gaspard, P. *J. Chem. Phys.* **1999**, *110*, 5619.

(62) Heisenberg, W. *Z. Phyz.* **1925**, *33*, 879.

(63) Jacobson, M. P.; Jung, C.; Taylor, H. S.; Field, R. W. *J. Chem. Phys.* **1999**, *111*, 600.

(64) Holme, T. A.; Levine, R. D. *J. Chem. Phys.* **1988**, *89*, 3380.

(65) Holme, T. A.; Levine, R. D. *Chem. Phys. Lett.* **1988**, *150*, 393.

(66) Holme, T. A.; Levine, R. D. *Chem. Phys.* **1989**, *131*, 169.

(67) Prosmiti, R.; Farantos, S. C. *J. Chem. Phys.* **1995**, *103*, 3299.

(68) Rose, J. P.; Kellman, M. E. *J. Chem. Phys.* **1995**, *103*, 7255.

(69) Mecke, R. *Z. Physik* **1933**, *81*, 313.

(70) Child, M. S.; Lawton, R. T. *Faraday Discuss.* **1981**, *71*, 273.

(71) Lawton, R. T.; Child, M. S. *Mol. Phys.* **1980**, *40*, 773.

(72) Henry, B. R.; Siebrand, W. *J. Chem. Phys.* **1968**, *49*, 5369.

(73) Siebrand, W.; Williams, D. F. *J. Chem. Phys.* **1968**, *49*, 1860.

(74) Child, M. S.; Halonen, L. *Adv. Chem. Phys.* **1984**, *57*, 1.

(75) Baggott, J. E. *Mol. Phys.* **1988**, *65*, 739.

(76) Lehmann, K. K. *J. Chem. Phys.* **1983**, *79*, 1098.

(77) Kellman, M. E. *J. Chem. Phys.* **1982**, *76*, 4528.

(78) Kellman, M. E. *J. Chem. Phys.* **1985**, *83*, 3843.

(79) Mills, I. M.; Robiette, A. G. *Mol. Phys.* **1985**, *56*, 743.

(80) Mills, I. M.; Mompean, F. J. *Chem. Phys. Lett.* **1986**, *124*, 425.

(81) Lehmann, K. K. *J. Chem. Phys.* **1986**, *84*, 6524.

(82) Della Valle, R. G. *Mol. Phys.* **1988**, *63*, 611.

(83) Lehmann, K. K. *J. Chem. Phys.* **1992**, *96*, 8117.

(84) Moss, D. B.; Duan, Z.-C.; Jacobson, M. P.; O'Brien, J. P.; Field, R. W. *J. Mol. Spectros.* **2000**, *199*, 265.

(85) Jacobson, M. P.; Silva, M. S.; Duan, Z.-C.; Field, R. W. Unpublished results.

(86) Jacobson, M. P. Ph.D. Thesis, Massachusetts Institute of Technology, 1999.

(87) Silva, M. S.; Jacobson, M. P.; Duan, Z.-C.; Field, R. W. In preparation.

(88) Levin, J.; Feldman, H.; Baer, A.; Ben-Hamu, D.; Heber, O.; Zajifman, D.; Vager, Z. *Phys. Rev. Lett.* **1999**, *81*, 3347.

(89) Avouris, P.; Gelbart, W. M.; El-Sayed, M. A. *Chem. Rev.* **1977**, *77*, 793.

(90) Keifer, J. H.; Mudipalli, P. S.; Wagner, A. F.; Harding, L. *J. Chem. Phys.* **1996**, *105*, 8075.

(91) Schork, R.; Köppel, H. *Theor. Chem. Acc.* **1998**, *100*, 204.

(92) The word recursion is used because a connection is made between measurements taken in independent experiments.

(93) Watson points out that the intensities he calculates are not, strictly speaking, Franck−Condon factors because the transition moment must be taken to be dependent on the bend angle in order to achieve reasonable results.